

Electronically controlled coherent linear optical sampling for optical coherence tomography

Stefan Kray,^{1*} Felix Spöler,¹ Thomas Hellerer,² and Heinrich Kurz¹

¹Institute of Semiconductor Electronics, RWTH Aachen University, Sommerfeldstr. 24, 52074 Aachen, Germany

²TOPTICA Photonics AG, Lochhamer Schlag 19, 82166 Gräfelfing, Germany

*kray@iht.rwth-aachen.de

Abstract: Electronically controlled coherent linear optical sampling for low coherence interferometry (LCI) and optical coherence tomography (OCT) is demonstrated, using two turn-key commercial mode-locked fiber lasers with synchronized repetition rates. This novel technique prevents repetition rate limitations present in previous implementations based on asynchronous optical sampling. Adjustable scanning ranges and scanning rates are realized within an interferometric setup by full electronic control of the mutual time delay of the two laser pulse trains. We implement this novel linear optical sampling scheme with broad spectral bandwidths for LCI, optical filter characterization and OCT imaging in two and three dimensions.

©2010 Optical Society of America

OCIS codes: (110.4500) Optical coherence tomography; (170.4500) Optical coherence tomography; (140.4050) Mode locked lasers; (040.2840) Heterodyne.

References and links

1. M. A. Duguay, and J. W. Hansen, "An ultrafast light gate," *Appl. Phys. Lett.* **15**(6), 192–194 (1969).
2. F. E. Lytle, R. M. Parrish, and W. T. Barnes, "An introduction to time-resolved pump probe spectroscopy," *Appl. Spectrosc.* **39**(3), 444–451 (1985).
3. G. C. Cho, W. Kütt, and H. Kurz, "Subpicosecond time-resolved coherent-phonon oscillations in GaAs," *Phys. Rev. Lett.* **65**(6), 764–766 (1990).
4. N. G. Chen, and Q. Zhu, "Rotary mirror array for high-speed optical coherence tomography," *Opt. Lett.* **27**(8), 607–609 (2002).
5. A. L. Oldenburg, J. J. Reynolds, D. L. Marks, and S. A. Boppart, "Fast-Fourier-domain delay line for in vivo optical coherence tomography with a polygonal scanner," *Appl. Opt.* **42**(22), 4606–4611 (2003).
6. R. A. McLaughlin, J. P. Williamson, M. J. Phillips, J. J. Armstrong, S. Becker, D. R. Hillman, P. R. Eastwood, and D. D. Sampson, "Applying anatomical optical coherence tomography to quantitative 3D imaging of the lower airway," *Opt. Express* **16**(22), 17521–17529 (2008).
7. T. Kanada, and D. L. Franzen, "Optical waveform measurement by optical sampling with a mode-locked laser diode," *Opt. Lett.* **11**(1), 4–6 (1986).
8. P. A. Elzinga, F. E. Lytle, Y. Jian, G. B. King, and N. M. Laurendeau, "Pump probe spectroscopy by asynchronous optical-sampling," *Appl. Spectrosc.* **41**(1), 2–4 (1987).
9. C. Janke, M. Först, M. Nagel, H. Kurz, and A. Bartels, "Asynchronous optical sampling for high-speed characterization of integrated resonant terahertz sensors," *Opt. Lett.* **30**(11), 1405–1407 (2005).
10. T. Yasui, Y. Kabetani, E. Saneyoshi, S. Yokoyama, and T. Araki, "Terahertz frequency comb by multifrequency-heterodyning photoconductive detection for high-accuracy, high-resolution terahertz spectroscopy," *Appl. Phys. Lett.* **88**(24), 241104 (2006).
11. A. Bartels, R. Cerna, C. Kistner, A. Thoma, F. Hudert, C. Janke, and T. Dekorsy, "Ultrafast time-domain spectroscopy based on high-speed asynchronous optical sampling," *Rev. Sci. Instrum.* **78**(3), 035107 (2007).
12. S. Schiller, "Spectrometry with frequency combs," *Opt. Lett.* **27**(9), 766–768 (2002).
13. F. Keilmann, C. Gohle, and R. Holzwarth, "Time-domain mid-infrared frequency-comb spectrometer," *Opt. Lett.* **29**(13), 1542–1544 (2004).
14. A. Schliesser, M. Brehm, F. Keilmann, and D. W. van der Weide, "Frequency-comb infrared spectrometer for rapid, remote chemical sensing," *Opt. Express* **13**(22), 9029–9038 (2005).
15. I. Coddington, W. C. Swann, and N. R. Newbury, "Coherent multiheterodyne spectroscopy using stabilized optical frequency combs," *Phys. Rev. Lett.* **100**(1), 013902 (2008).
16. C. Dorrer, D. C. Kilper, H. R. Stuart, G. Raybon, and M. G. Raymer, "Linear optical sampling," *IEEE Photon. Technol. Lett.* **15**(12), 1746–1748 (2003).
17. S. J. Lee, B. Widiyatmoko, M. Kourogi, and M. Ohtsu, "Ultrafast scanning speed optical coherence tomography using optical frequency comb generators," *Jpn. J. Appl. Phys.* **40**(Part 2, No. 8B), L878–L880 (2001).
18. S. Kray, F. Spöler, M. Först, and H. Kurz, "Dual femtosecond laser multiheterodyne optical coherence tomography," *Opt. Lett.* **33**(18), 2092–2094 (2008).

19. I. Coddington, W. C. Swann, L. Nenadovic, and N. R. Newbury, "Rapid and precise absolute distance measurements at long range," *Nat. Photonics* **3**(6), 351–356 (2009).
20. I. Coddington, W. C. Swann, and N. R. Newbury, "Coherent linear optical sampling at 15 bits of resolution," *Opt. Lett.* **34**(14), 2153–2155 (2009).
21. B. L. Danielson, and C. D. Whittenberg, "Guided-wave reflectometry with micrometer resolution," *Appl. Opt.* **26**(14), 2836–2842 (1987).
22. D. Huang, E. A. Swanson, C. P. Lin, J. S. Schuman, W. G. Stinson, W. Chang, M. R. Hee, T. Flotte, K. Gregory, C. A. Puliafito, and J. G. Fujimoto, "Optical coherence tomography," *Science* **254**(5035), 1178–1181 (1991).
23. J. Welzel, E. Lankenau, R. Birngruber, and R. Engelhardt, "Optical coherence tomography of the human skin," *J. Am. Acad. Dermatol.* **37**(6), 958–963 (1997).
24. W. C. Swann, J. J. McFerran, I. Coddington, N. R. Newbury, I. Hartl, M. E. Fermann, P. S. Westbrook, J. W. Nicholson, K. S. Feder, C. Langrock, and M. M. Fejer, "Fiber-laser frequency combs with subhertz relative linewidths," *Opt. Lett.* **31**(20), 3046–3048 (2006).
25. F. Tauser, C. Rausch, J. H. Posthumus, and F. Lison, "Electronically controlled optical sampling using 100 MHz repetition rate fiber lasers," *Proc. SPIE* **6881**, 68810O (2008).
26. F. Spöler, S. Kray, P. Grychtol, B. Hermes, J. Bornemann, M. Först, and H. Kurz, "Simultaneous dual-band ultra-high resolution optical coherence tomography," *Opt. Express* **15**(17), 10832–10841 (2007).
27. S. Kray, F. Spöler, M. Först, and H. Kurz, "High-resolution simultaneous dual-band spectral domain optical coherence tomography," *Opt. Lett.* **34**(13), 1970–1972 (2009).
28. S. T. Cundiff, and J. Ye, "Colloquium: Femtosecond optical frequency combs," *Rev. Mod. Phys.* **75**(1), 325–342 (2003).
29. S. T. Cundiff, "Phase stabilization of ultrashort optical pulses," *J. Phys. D Appl. Phys.* **35**(8), R43–R59 (2002).
30. F. Tauser, A. Leitenstorfer, and W. Zinth, "Amplified femtosecond pulses from an Er:fiber system: nonlinear pulse shortening and selfreferencing detection of the carrier-envelope phase evolution," *Opt. Express* **11**(6), 594–600 (2003).
31. M. Hofer, M. E. Fermann, F. Haberl, M. H. Ober, and A. J. Schmidt, "Mode locking with cross-phase and self-phase modulation," *Opt. Lett.* **16**(7), 502–504 (1991).
32. I. Horcas, R. Fernández, J. M. Gómez-Rodríguez, J. Colchero, J. Gómez-Herrero, and A. M. Baro, "WSXM: a software for scanning probe microscopy and a tool for nanotechnology," *Rev. Sci. Instrum.* **78**(1), 013705 (2007).
33. A. F. Fercher, C. K. Hitzenberger, G. Kamp, and S. Y. Elzaiat, "Measurement of intraocular distances by back-scattering spectral interferometry," *Opt. Commun.* **117**(1-2), 43–48 (1995).
34. G. Häusler, and M. W. Lindner, "'Coherence radar' and 'spectral radar'—new tools for dermatological diagnosis," *J. Biomed. Opt.* **3**(1), 21–31 (1998).
35. S. R. Chinn, E. A. Swanson, and J. G. Fujimoto, "Optical coherence tomography using a frequency-tunable optical source," *Opt. Lett.* **22**(5), 340–342 (1997).
36. U. H. P. Haberland, V. Blazek, and H. J. Schmitt, "Chirp optical coherence tomography of layered scattering media," *J. Biomed. Opt.* **3**(3), 259–266 (1998).
37. B. Potsaid, I. Gorczynska, V. J. Srinivasan, Y. L. Chen, J. Jiang, A. Cable, and J. G. Fujimoto, "Ultrahigh speed spectral / Fourier domain OCT ophthalmic imaging at 70,000 to 312,500 axial scans per second," *Opt. Express* **16**(19), 15149–15169 (2008).
38. A. F. Fercher, W. Drexler, C. K. Hitzenberger, and T. Lasser, "Optical coherence tomography - principles and applications," *Rep. Prog. Phys.* **66**(2), 239–303 (2003).
39. G. Sucha, M. E. Fermann, D. J. Harter, and M. Hofer, "A new method for rapid temporal scanning of ultrafast lasers," *IEEE J. Sel. Top. Quantum Electron.* **2**(3), 605–621 (1996).
40. P. Giaccari, J. D. Deschênes, P. Saucier, J. Genest, and P. Tremblay, "Active Fourier-transform spectroscopy combining the direct RF beating of two fiber-based mode-locked lasers with a novel referencing method," *Opt. Express* **16**(6), 4347–4365 (2008).

1. Introduction

In optical sampling, a transient waveform under study is gated with time delayed laser pulses, sampling this waveform with high time resolution. This technique is commonly employed for exploiting nonlinear optical effects [1] and for pump probe studies [2,3]. However, in these approaches the overall measurement time and scanning range is strongly limited by mechanical scanning of the time delay of the probe pulses. Although frequencies of tens of kHz for sweeping the scanning range, named as scanning rate f_ϕ within this work, have been reported, the scanning range is limited to a few centimeters and the signal to noise ratio can degrade due to mechanical instabilities [4–6].

These limitations can be overcome by asynchronous optical sampling (ASOPS), where two pulsed lasers with slightly detuned repetition rates are employed [7,8]. A constant difference Δf_{REP} between the repetition rates of two lasers leads to an increasing mutual time delay. Thus, the pulses of the first laser sweep the pulses of the second laser, performing a non-mechanical scan of the time delay. ASOPS has been demonstrated for non-mechanical mea-

measurements of time domain transients [7,8], for probing integrated sensors [9], for terahertz- and infrared spectroscopy [10–15], for linear optical sampling [16], for coherent linear detection in LCI and OCT [17,18], and recently for precise distance- and dispersion measurements [19,20]. In the coherent ASOPS implementations, such as LCI and OCT, the electric fields of the first laser pulse train sweep the electric field of the second laser pulse train. In LCI, a sample under investigation is probed with light of low temporal coherence and interfered with a second, time delayed low coherence beam [21]. The extension to OCT imaging is achieved by two-dimensional scanning. Cross-sectional images of the sample are obtained by displaying the logarithmic amplitude of the depth dependent correlation signals [22].

The ASOPS technique restricts the maximum temporal delay between the two laser pulse trains to f_{REP}^{-1} , given by the overall laser repetition rate f_{REP} . This maximum temporal delay corresponds to a fixed spatial scanning range z_{MAX} within interferometric setups, given by $z_{\text{MAX}} = c_0 / (2 \cdot n \cdot f_{\text{REP}})$ with c_0 as speed of light and n as average refractive index of the scanning range. For a 1 GHz repetition rate laser and measurements in free space ($n = 1$) this scanning range corresponds to 0.15 meters. However, a ten times lower repetition rate already increases the scanning range to 1.5 meters. Although large scanning ranges might be advantageous for several applications, the whole scanning range has to be measured in every single scan. In biological samples, the visualizable depth strongly depends on the absorption and scattering properties. In case of biological tissue, the visualizable depth by coherent detection with infrared light does not exceed 1-2 mm [23]. In further applications, e.g. subsurface analysis for part inspection, only a small region within a large scanning range might be of interest. Thus, ASOPS applied to coherent linear optical sampling for a region of interest of 2 mm wastes >99% of the data acquisition time and memory for a 100 MHz repetition rate laser.

The scanning rate f_{ϕ} is given by the difference of the repetition rates $f_{\phi} = \Delta f_{\text{REP}} = f_{\text{REP}2} - f_{\text{REP}1}$ for the ASOPS technique. As we will discuss below, the scanning rate for LCI and OCT imaging is restricted by the discrete nature of the pulse timings: a minimum amount of three pulses per coherence length is necessary for adequate sampling of the correlation signal. Thus, the scanning rate of ASOPS is significantly limited by the overall pulse repetition rate and the coherence length of the light source.

These limitations can be partly relaxed by using lasers with high repetition rates >1 GHz [18]. Although these high repetition rate lasers are commercially available, they often require free space cavities and a separate pump source, limiting the possible range of applications to laboratory operation. Contrarily, commercial mode-locked fiber lasers allow flexible setups and stable turn-key operation even in industrial or clinical environments and have lower costs. However, the fiber based design demands higher cavity lengths in the range of several meters, limiting the repetition rate to ≈ 100 MHz. The resulting scanning ranges of 1.5 m and the fundamentally limited scanning rates of 350 Hz (discussed below) prohibit useful operation. Furthermore, these lasers are individually pumped by distinct pump sources, leading to different behaviors of the carrier envelope offsets (CEOs). Interferometric application of distinct fiber lasers has been demonstrated so far using non-linear conversion to cancel the CEO frequencies [13] or sophisticated stabilization schemes to lock the resulting frequency combs [19,24]. These methods either require high power lasers for non-linear conversion or additional light sources for stabilization, inevitably increasing complexity and costs of the setup.

To overcome these limitations, we adapt an alternative scanning scheme, known as electronically controlled optical sampling (ECOPS) [25] for the first time to coherent linear optical sampling. ECOPS differs from other techniques by directly controlling the mutual time delay of the laser pulse trains, using a high bandwidth feedback loop with low timing jitter [25]. The laser pulses are measured by photodiodes, the phase difference of the pulses is determined and locked tightly to a user adjustable phase signal by controlling the laser repetition rates. The signal applied is directly proportional to the time delay, allowing enhanced control options. The scanning range, rate and offset (the starting point of the scanning range) can be chosen individually by setting the appropriate electronic parameters. Thus, the repetition rate limitations of the scanning range and scanning rate by the ASOPS technique are eliminated. Owing to the short pulse lengths and the inherent broad spectral bandwidths of the lasers, we

permit the application of long cavity fiber based lasers in combination with virtually no mechanical scanning in the depth direction for time domain low coherence interferometry. Our technique demands only a stabilization of the repetition rates, significantly simplifying the overall setup compared to previous works [20]. The potential of this flexible technique beyond ASOPS is shown. SNR enhancement by averaging for LCI, optical filter characterization and OCT imaging in two and three dimensions is demonstrated.

2. Repetition rate limitations of coherent linear optical sampling

In coherent linear optical sampling, the electric field of a light source is interferometrically overlapped with a second, time delayed electric field. This sweep of the electric fields generates correlation signals. Although this technique does not require pulsed lasers, these light sources are commonly employed due to their low noise operation and low coherence lengths resulting from the broad spectral bandwidths. However, as we will show here, the discrete nature of the laser pulse timings can limit the generation of the correlation signals in time domain systems significantly.

Figures 1(a) and 1(b) show single frames of the corresponding movie sequences ([Media 1](#) and [Media 2](#), respectively) of the generation of correlation signals. Two animations were generated by simulating different scanning velocities of a reference mirror within a time domain setup. Figure 1(a) was obtained for $v = 7.5$ m/s, Fig. 1(b) represents simulated data for $v = 500$ m/s. The other laser parameters were chosen according to the laser system employed. The repetition rate corresponds to $f_{\text{REP}} = 100$ MHz. A transform limited spectral bandwidth of $\Delta\lambda = 70$ nm FWHM (corresponding to 50 fs pulse length) at a center wavelength of $\lambda = 1550$ nm was assumed.

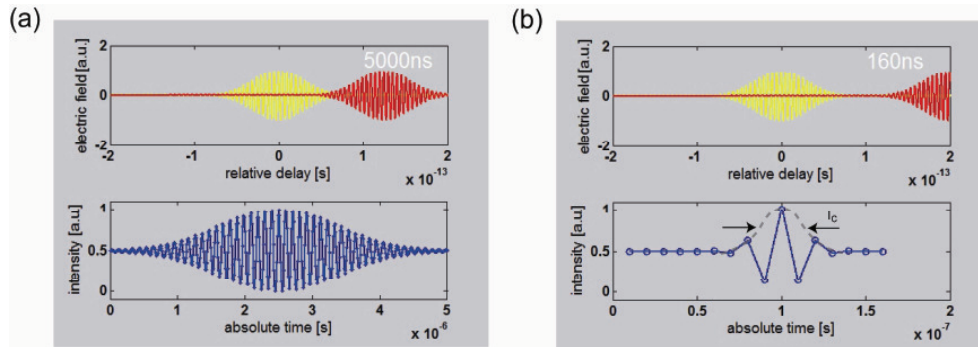


Fig. 1. Generation of correlation signals with (a) $v = 7.5$ m/s ([Media 1](#)) and (b) $v = 500$ m/s ([Media 2](#)). The simulation data was obtained for a pulsed laser with a repetition rate of $f_{\text{REP}} = 100$ MHz and a spectral bandwidth of $\Delta\lambda = 70$ nm FWHM.

Figure 1 emphasizes the limitations in scanning velocity due to the discrete nature of the laser pulse timings. The correlation signal obtained with the lower scanning velocity comprises several hundred laser pulses, while the second correlation signal in Fig. 1(b) contains only 20 laser pulses. The coherence length, determined as the full width at half maximum value of the correlation signal, consists of a minimum amount of three laser pulses. Fewer pulses per coherence length would not generate a carrier frequency within the envelope, necessary for heterodyne detection.

Obviously the maximum achievable scanning velocity v depends on the pulse delay τ (given by the laser repetition rate $f_{\text{REP}} = 1/\tau$) and on the coherence length l_c of the light source. Assuming the minimum amount of three pulses per coherence length, the scanning velocity is limited to:

$$v \leq \frac{l_c}{3 \cdot \tau} = \frac{l_c \cdot f_{\text{REP}}}{3}. \quad (1)$$

The limit of $v = 523$ m/s for the laser system employed here cannot be reached with mechanical scanning delay lines. However, this scanning velocity is easily achievable with asynchronous optical sampling, using two pulsed lasers with detuned repetition rates. In ASOPS, the scanning range z_{\max} is swept with the scanning velocity v , having a scanning rate corresponding to the difference frequency Δf_{REP} :

$$\Delta f_{\text{REP}} = \frac{v}{z_{\max}} \leq \frac{2 l_c \cdot f_{\text{REP}}^2}{3 c_0}. \quad (2)$$

Hence, the ASOPS difference frequency Δf_{REP} is limited by the square of the laser repetition rate, giving a maximum value of $\Delta f = 349$ Hz for the laser system employed. This limits the maximum A-Scan rate $f\phi = \Delta f_{\text{REP}}$ to only 349 scans per second.

Figure 2(a) analyzes the maximum achievable scanning rates as a function of the repetition rate, using coherent detection with ASOPS. The calculations were performed for three different coherence lengths, corresponding to achievable resolutions in OCT imaging with different commercial light sources. The coherence length of $l_c = 15.7 \mu\text{m}$ represents the resolution achieved in this study, using fiber lasers with 100 MHz repetition rate. In our previous work, a resolution of $8 \mu\text{m}$ was obtained with a free space high repetition rate laser with $f_{\text{REP}} = 1$ GHz [18]. A resolution of $l_c = 1.7 \mu\text{m}$ has been demonstrated in time domain OCT with a low repetition rate commercial supercontinuum (SC) laser with $f_{\text{REP}} = 20$ MHz [26]. The corresponding values for the three repetition rates and coherence lengths are indicated by the colored dashed lines.

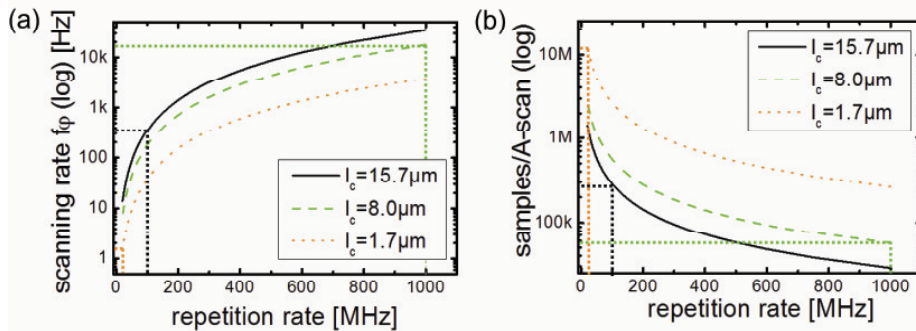


Fig. 2. Scanning rate $f\phi$ and samples/A-scan in dependence of the overall laser repetition rate of ASOPS scanning. All curves are plotted for three different coherence lengths of $l_c = 15.7$, 8.0 and $1.7 \mu\text{m}$. The perpendicular colored dashed lines correspond to the parameters of the three commercial light sources mentioned above.

While ASOPS allows outstanding scanning rates of $f\phi > 10\text{kHz}$ and scanning velocities beyond sonic velocity with high repetition rate lasers of $f_{\text{REP}} = 1$ GHz (dashed green line) [18], $f\phi$ is limited to only 349 Hz for $f_{\text{REP}} = 100$ MHz here (dashed black line), although the coherence length is slightly higher. ASOPS suffers dramatically from low repetition rate lasers, such as commercial SC sources (dashed orange line), commonly employed for ultrahigh resolution OCT imaging [26,27]. The calculated scanning rate for a SC light source, having a repetition rate of 20 MHz and a coherence length below $1.7 \mu\text{m}$ is limited to only 1.5 A-scans per second.

Figure 2(b) visualizes the amount of samples/A-scan, which have to be measured due to the fixed scanning range. The amount ranges from some kSamples/A-scan for high repetition rate systems to $>10\text{MSamples/A-scan}$ for the SC light source. Here, a predominant amount of data acquisition time and memory is wasted, if only a specific region within an A-scan is of interest.

Hence, the ASOPS approach is not scalable and cannot be applied usefully to repetition rates $\ll 1\text{GHz}$. A new approach is needed to bridge the gap between time domain systems

based on rapid scanning optical delay lines, which cover only small scanning ranges, and ASOPS based systems covering only a fixed large scanning range.

3. Operation principle

The limitations discussed above are circumvented by breaking the stringent necessity of equal scanning rate and difference frequency $f_\phi = \Delta f_{\text{REP}}$, given by the ASOPS technique. This is achieved by applying a user selectable phase control signal $\phi(t)$ for direct control of the mutual time delay between two laser pulse trains [25]. The phase signal instantaneously modifies the repetition rate of one laser, leading to a time dependent difference $\Delta f_{\text{REP}} = f_{\text{REP}2} - f_{\text{REP}1}$ in the repetition rates. The derivative of the phase signal $d\phi/dt$ is proportional to the instantaneous difference frequency $\Delta f_{\text{REP}}(t)$. Hence the phase signal $\phi(t)$ is directly proportional to the resulting time delay and corresponds to a scanning delay line in time domain low coherence interferometry. The peak to peak amplitude is equal to the maximum mechanical delay, which is scanned with a scanning rate $f_\phi > |\Delta f_{\text{REP}}(t)|$. A constant offset of the phase signal fixes the time delay of the pulses to a constant value, corresponding to an arbitrary offset within the scanning range; i. e. the zero-point of the mechanical delay is set by applying zero voltage.

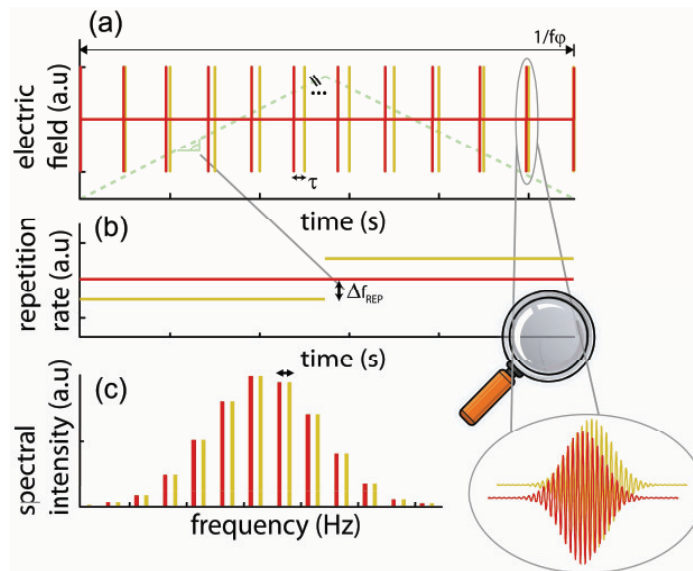


Fig. 3. : Operation principle of electronically controlled coherent linear optical sampling. (a) Pulse trains of both lasers (solid red and yellow lines) in dependence of the phase control signal $\phi(t)$ (dashed green line). The mutual pulse delay τ is determined by the phase signal. The pulse delay increases or decreases, depending on the sign of the phase signal slope. The zero-point is reached again after the full cycle time $1/f_\phi$. Inset: electric fields of the pulses. (b) Repetition rate change Δf_{REP} in dependence of the phase control signal. (c) Frequency domain picture of the resulting (time dependent) frequency combs. Neighboring modes of the combs are separated by a difference frequency, depending on the slope of the phase signal, the laser repetition rates and the individual carrier envelope offset frequencies.

The described properties are visualized in Fig. 3(a), sketching the phase control signal applied (dashed green line) and the resulting timings of the laser pulses (solid red and yellow lines). The sweeping electric fields of the laser pulses, indicated by the inset in Fig. 3(a), generate correlation signals within an interferometric setup. The repetition rates of both lasers are sketched in Fig. 3(b). Mechanical action within the cavity of laser 1 is required only for a changing slope of the phase control signal. Figure 3(c) shows the resulting frequency domain picture for both lasers. Each pulse train forms an optical frequency comb, having mode frequencies at $n \cdot f_{\text{REP}} + f_{\text{CEO}}$ with an integer number n , the repetition rate f_{REP} , and a carrier envelope offset frequency f_{CEO} [28]. Two neighboring modes of the frequency combs generate

heterodyne beat signals on the photodetector within the interferometric setup. The sum signal of the modes is filtered out and only the difference frequency for each comb mode remains, forming a beat signal f_{BEAT} in the radio frequency domain:

$$f_{\text{BEAT}} = (nf_{\text{REP}2} + f_{\text{CEO}2}) - (nf_{\text{REP}1} + f_{\text{CEO}1}) = (n\Delta f_{\text{REP}}(t) + \Delta f_{\text{CEO}}). \quad (3)$$

Assuming similar overall cavity lengths z_c and group velocities v_g (the overall repetition rates are equal), the difference frequency $\Delta f_{\text{REP}}(t)$ depends on the change in cavity length $\Delta z(t)$ within the cavity length tunable laser 1:

$$\Delta f_{\text{REP}}(t) = \frac{v_g}{z_c} - \frac{v_g}{z_c + \Delta z(t)} \approx \frac{v_g \Delta z(t)}{z_c^2} = f_{\text{REP}} \frac{\Delta z(t)}{z_c}. \quad (4)$$

Thus, a small cavity length change of $\Delta z = 10.5\mu\text{m}$ (0.0035 % of the cavity length) is sufficient to reach the maximum time domain scanning rate of $\Delta f_{\text{REP}} = 349$ Hz here with an overall repetition rate of $f_{\text{REP}} = 100\text{MHz}$. This cavity length change can be achieved easily with standard piezoelectric transducers. Even rapid variations of the cavity length change within this small range do not have an impact on the stability of the laser. The frequency f_{CEO} results from the pulse to pulse phase slip of the carrier within the pulse envelope. It depends on the group velocity v_g and phase velocity v_p within the laser cavity:

$$f_{\text{CEO}} = \frac{\omega_c v_g}{2\pi} \left(\frac{1}{v_g} - \frac{1}{v_p} \right), \quad (5)$$

with ω_c as angular center frequency of the comb (see [29] for details). Thus, the cavity length tuning does not influence the offset frequency, as an identical phase and group velocity can be assumed within the free-beam tuning section of the laser and therefore the dispersion of the laser cavity is not changed. However, the stability of f_{CEO} critically depends on stable dispersion conditions of the two lasers. Small variations of the pulse to pulse phase slip degrade the carrier frequency and thus the signal to noise ratio of coherent linear optical sampling. Hence, stable light sources are important requirements for avoiding a fringe washout due to CEO jitter. This fact becomes particularly important, when different pump sources are used, causing individual CEO jitter in each laser.

4. Methods

Figures 4(a) and 4(b) sketch the optical and electrical setup for electronically controlled coherent linear optical sampling, respectively. Figure 4(c) shows the setup of the fiber lasers.

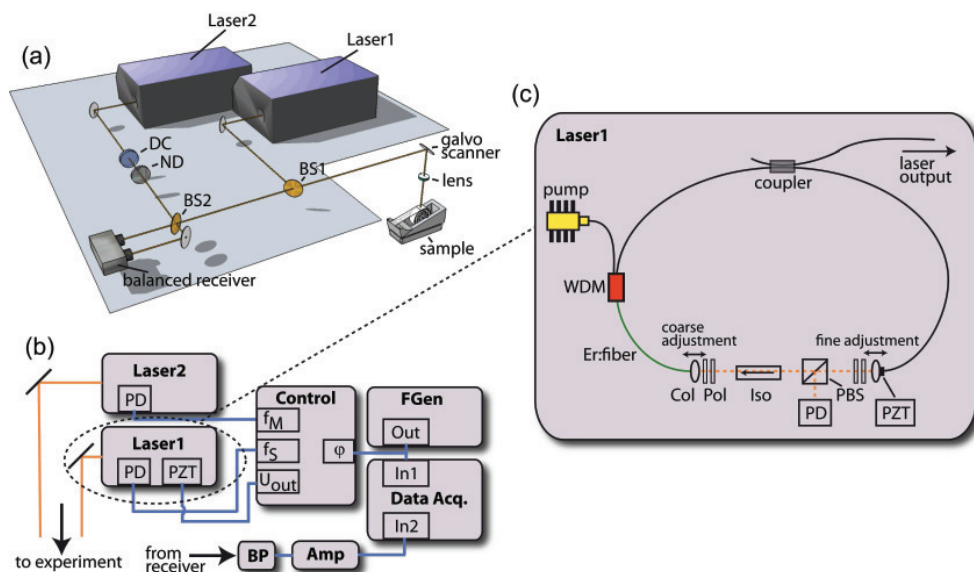


Fig. 4. (a) Optical setup of the experiment. DC: dispersion compensation, ND: neutral density filter, BS: beamsplitter. (b) Electrical setup for the laser control. PD: photo detector, PZT: piezoelectric transducer, f_M : frequency of the master laser, f_S : frequency of the slave laser, U_{out} : piezoelectric transducer voltage output, ϕ : phase input, FGen: frequency generator, BP: band-pass filter, Amp: analog logarithmic amplifier. (c) Setup of the commercial fiber laser. WDM: wavelength division multiplexing, Er: fiber: erbium doped fiber, Pol: polarization control, Iso: isolator, PBS: polarizing beam splitter, Col: fiber collimator

Two commercial femtosecond fiber lasers (FFS.BU, Toptica Photonics AG, Germany) are arranged within an interferometer setup. Each laser contains a ring oscillator with an erbium doped fiber amplifier [30]. An essential part of the oscillator is a free-beam section comprising several waveplates and a polarizer, serving as artificial saturable absorber. Hence, mode-locking is achieved by nonlinear polarization evolution via the optical Kerr effect [31].

Laser 2 (the master oscillator) runs freely with a repetition rate of 100MHz, laser 1 (the slave oscillator) can be tuned in repetition rate by varying the length of the free-beam section. A stepper motor and a piezoelectric transducer within the cavity of this laser are used for coarse and fine adjustment, respectively. The change in cavity length results in a modified repetition rate and thus in different timing delays of the laser pulses. A master slave lock is realized by matching the repetition rate of the slave oscillator to the free running master oscillator, using a phase locked loop (PLL) circuit (FFS.SYS-SYNC-PLL, Toptica Photonics AG, Germany). The phase difference of both pulse trains is determined by measuring the laser pulses with internal photo diodes. The phase difference serves as error signal, which is coupled back to the piezoelectric transducer. The stepper motor is only activated for compensation of larger drifts of the cavity length. Varying the delay between the two pulse trains is achieved by electronically sweeping the set point of the locking electronics: an additional input signal $\phi(t)$ is added to the determined phase difference before the feedback loop is closed (see [25] for details). A linearly sweeping phase- and time delay is accomplished by applying a triangular function as input signal. The amplitude, offset and frequency of the sweeping time delay scales with $\phi(t)$.

In the ideal case of no external disturbances of the cavity length, an increasing time delay relative to the master laser results from a constant, slightly higher cavity length of the slave laser. When the maximum time delay is reached, the cavity length of the slave laser has to be switched below the cavity length of the master laser for achieving a decreasing time delay [see Fig. 3(b)]. Thus, the main advantage of ECOPS beyond ordinary mechanical scanning results from the fact that mechanical action is only required for changing the slope of the time delay.

Only slight mechanical movements in the range of some micrometers are necessary for appropriate changes of the cavity length. In this manner the electronically controlled delay can be used for fast and flexible optical sampling.

The setup of this technique for application in coherent linear optical sampling is shown in Fig. 4(a). The output of laser 1 is guided to the sample by beamsplitter 1. A galvanometer scanner deflects the beam for two-dimensional scanning; a lens is used for focusing the light onto the sample. The backscattered light of the sample arm is interferometrically overlapped at beamsplitter 2 with the light of laser 2. The dispersion of both lasers is matched by an optical windows applied as dispersion compensation DC, the reference arm intensity is reduced by a neutral density filter ND. The interferometric signal is detected with a balanced receiver, bandpass filtered and optionally demodulated by an analog logarithmic amplifier. The received signal and the phase control signal are measured by a multichannel transient recorder (Saturn, AMO GmbH, Germany). A subsequent numerical post processing step renders the data to images.

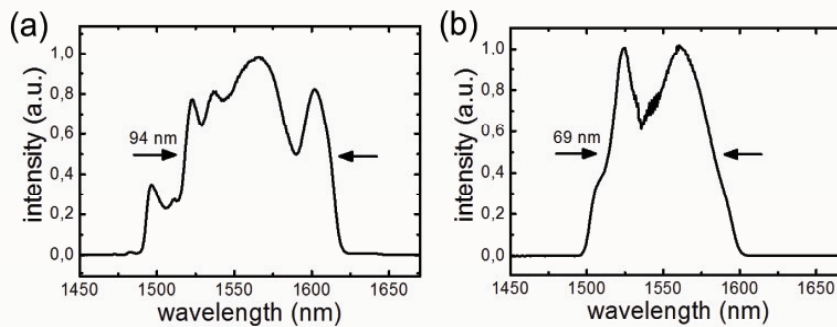


Fig. 5. Output spectra of (a) laser 1 (slave laser) and (b) laser 2 (master laser), respectively. The full widths at half maximum spectral bandwidths were determined to be 94 and 69 nm, respectively.

Figure 5 shows the optical output spectra of both fiber lasers. The optical spectrum of laser 1 is centered at 1560 nm and has 94 nm full width at half maximum (FWHM) spectral bandwidth. The second laser spectrum is centered at 1550 nm with 69 nm FWHM bandwidth. In OCT, the axial resolution is defined by the coherence length of the light source and thus by the spectral bandwidth, or in this case, by the spectral overlap of both lasers. The expected axial resolution is limited by the smaller spectral bandwidth of the second laser, calculated to be 15.4 μm FWHM. The lateral resolution was calculated to be 20 μm FWHM. The output power was measured to be 8.4 mW for the first laser and 4.6 mW for the second laser. The sensitivity of the method, defined as the lowest sample arm signal distinguishable from the noise, was measured to be -81 dB for 2.6 mW sample arm power by determining the sample arm attenuation with a mirror as sample for reaching a SNR of 1. The dynamic range achieved using an analog logarithmic amplifier followed by the A/D conversion was measured to be 75dB by determining the ratio of maximum to minimum optical sample arm signal without saturating the detection electronics.

5. Results

5.1 SNR enhancement by averaging for low coherence interferometry

A coverslip within the sample arm was imaged with the objective to test the capabilities for low coherence interferometry. The zero-point within the scanning range was set close to the coverslips by adjusting the electronic signal delay for the PLL control.

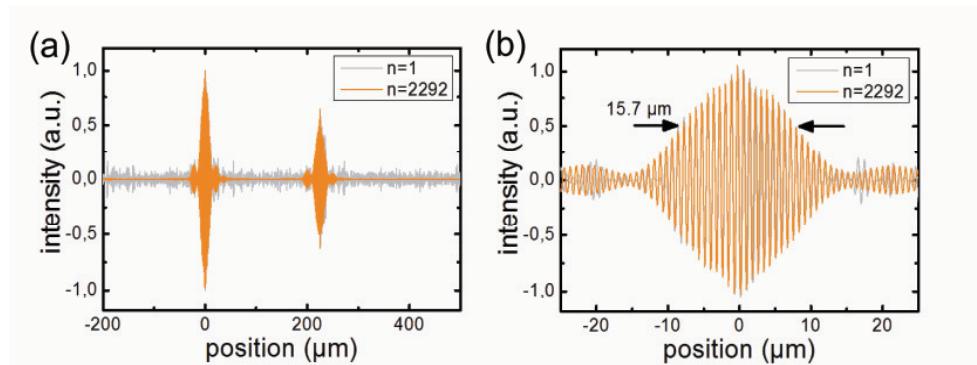


Fig. 6. LCI scans of a coverslip, measured with $f_{\phi} = 492$ Hz. The gray curves show a single measurement, orange curves represent averaged signals. (a) Correlation signal of the air-glass and glass-air interface of the coverslip. (b) Magnification of the air-glass interface of the correlation signal.

The Figs. 6(a) and 6(b) represent the resulting correlation signals. The curves in gray represent single measurements, the curves in orange show averaged scans. The signals were obtained for an overall scanning range of 18 mm and a scanning rate of $f_{\phi} = 492$ Hz. Such a scanning rate is not possible with the ASOPS technique due to the repetition rate limitations discussed in section 2.

A jitter correction procedure was applied to remove low frequency timing jitter caused by imperfections of the stabilization electronics. Slight deviations in the repetition rates lead to fluctuations in the time delay of the laser pulses. Timing jitter is determined as deviation from the true time delay to the intended time delay given by the phase control signal. As discussed elsewhere, timing jitter accumulates and scales linearly with the time elapsed after the trigger event (zero point of the phase control signal) [11]. Instabilities working on slow time scales dominate and give rise to offset shifts of the correlation signals. The coverslip signals do not appear at perfectly equidistant time offsets and therefore cancel out in the averaging process. This effect is avoided by detecting the correlation peaks and determining their median position from several scans. The position deviations of the coverslip signal within all A-Scans were measured to be $56.5 \mu\text{m}$ FWHM with a scanning velocity >8 m/s. This timing jitter of 188 fs FWHM is accumulated over the A-scan time of 2 ms. The individual position fluctuations are interpreted as measure for the jitter per A-scan and shifted to the median position by an interpolation procedure. A consecutive Hilbert transformation permits separate averaging of amplitude and phase information, further reducing the fringe washout.

A number of $n = 2292$ single axial scans was used for averaging the correlation signals in Figs. 6(a) and 6(b), limited by the memory of the data acquisition system. All curves are normalized to the maximum peak amplitude. Figure 6(b) shows the air-glass interface, which is the entrance signal of the coverslip. The axial resolution of the system was determined by measuring the full width at half maximum value of the correlation signal. The FWHM resolution of the correlation signal in Fig. 6(b) gives an axial resolution of $15.7 \mu\text{m}$. The increase in signal to noise ratio was measured by determining the individual SNRs of the single and averaged scans. The measured SNR advantage of the averaged signal equals the theoretical noise advantage factor of $\sqrt{2292} = 47.8$. Although the fiber lasers are pumped by different pump sources, the carrier frequency is stable within 1.6% standard deviation and allows fringe averaging of consecutive scans for SNR enhancement.

5.2 Optical response characterization

Signal averaging can be employed for characterizing optical response functions. Figure 7 shows the time- and frequency domain characteristics of an optical filter within the sample arm.

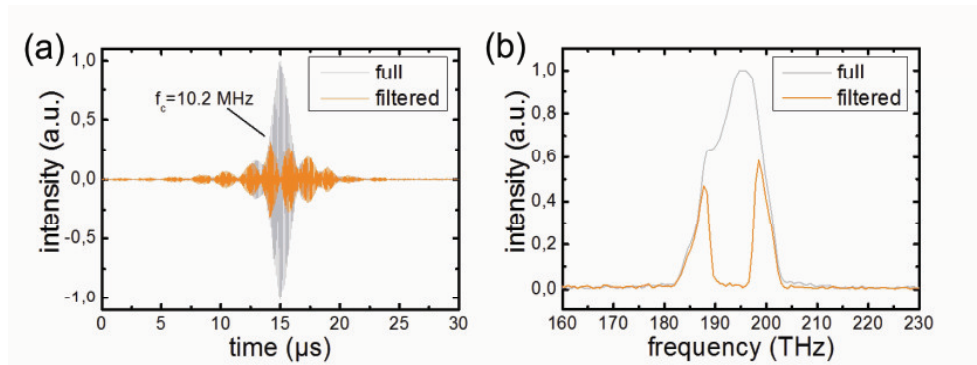


Fig. 7. Time- and frequency domain response of an optical bandstop filter, measured with $f_c = 51$ Hz. (a) Time domain transient of the full (gray) and filtered (orange) spectral bandwidth. (b) Corresponding frequency domain response.

Figure 7(a) highlights the time domain response of an optical bandstop filter, placed within the sample arm. A wavelength region around the central wavelength of the lasers is filtered out by blocking parts of the spectrum within a grating lens based spatial filter. The signal in gray represents the averaged correlation function with full spectral bandwidth. The orange overlay results after filtering the sample arm. The correlation function is apparently broadened and split to several sidelobes. The carrier frequency of the correlation signal was measured to be 10.2 MHz and corresponds to the center frequency of the frequency combs in the optical domain. Thus, a scaling factor of 1.9×10^7 was used to scale the Fourier transformation of the correlation signal to the optical domain, shown in Fig. 7(b). The missing frequencies arising from the bandstop filter are clearly evident.

5.3 Two- and three dimensional optical coherence tomography

An extension of the method to optical coherence tomography is possible by using a galvanometer scanner and a lens within the sample arm. The sample arm lens focuses the laser to a spot, which is translated by the galvanometer scanner. Two-dimensional images are achieved by synchronizing the galvanometer scanner to the axial scanning process. Jitter correction was performed by setting a coverslip as reference point within the scanning range. The coverslip signal was used for eliminating low frequency jitter by shifting the individual A-scans to their correct position. Further jitter compensation is possible by applying a software filter [18].

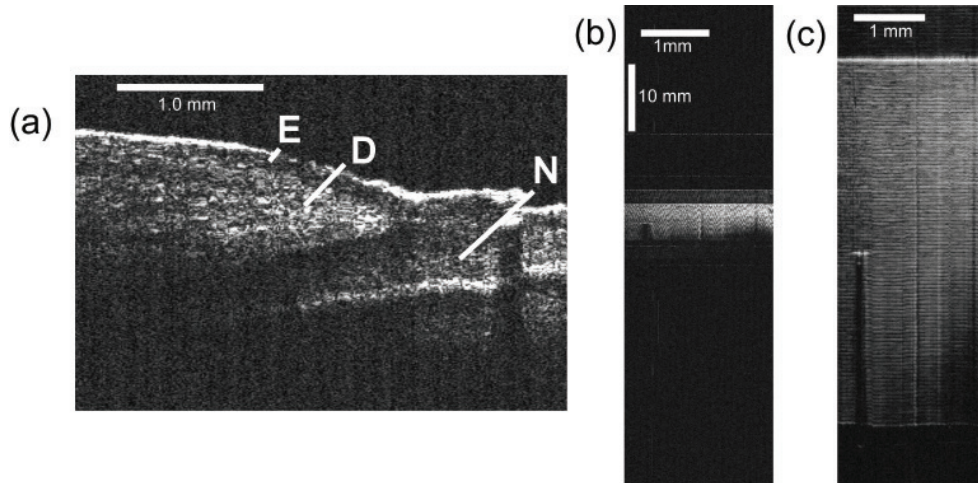


Fig. 8. Two-dimensional OCT images of (a) a human nail fold (3.3 mm width x 2.3 mm height) measured with $f_{\phi} = 52$ Hz, (b) an adhesive tape role (2.25 mm width x 72 mm height) and (c) magnified region of the adhesive tape role (2.25 mm width x 7 mm height), measured with $f_{\phi} = 37$ Hz. E: epidermis, D: dermis, N: nail plate. The scale bar in (b) corresponds to 1 mm in horizontal and 10 mm in vertical direction.

Figure 8 demonstrates optical coherence tomography by imaging a biological and a technical sample, respectively. Figure 8(a) shows a human nail fold, measured in vivo using 2.6mW sample arm power. The epidermal layers (E) can be discriminated from the lower dermal layer (D). The nail plate (N) is observable, emerging from under the cuticle. Figure 8(b) shows an adhesive tape role within a scanning range of 72 mm, Fig. 8(c) represents a magnified region of Fig. 8(b). The individual layers of the tape role can be easily identified. Hence, the method is suitable for biomedical as well as technical applications.

The flexibility of an adjustable scanning range can be used for extending our method to three dimensional surface inspection tasks. A mechanical translation stage is used to scan a coin perpendicular to the galvanometer movement. This coin was located 17 mm above a reflecting surface. Figure 7 demonstrates the high depth resolution within a large scanning range. The overall dimensions of the measured volume are 9 mm width x 8.7 mm height x 122mm depth. The volume data consists of approximately 100x100 depth scans with a total measurement data size of 1GB. Although the scanning range is quite large, the memory consumption is still a factor of 12 below the size needed for ASOPS based measurements.

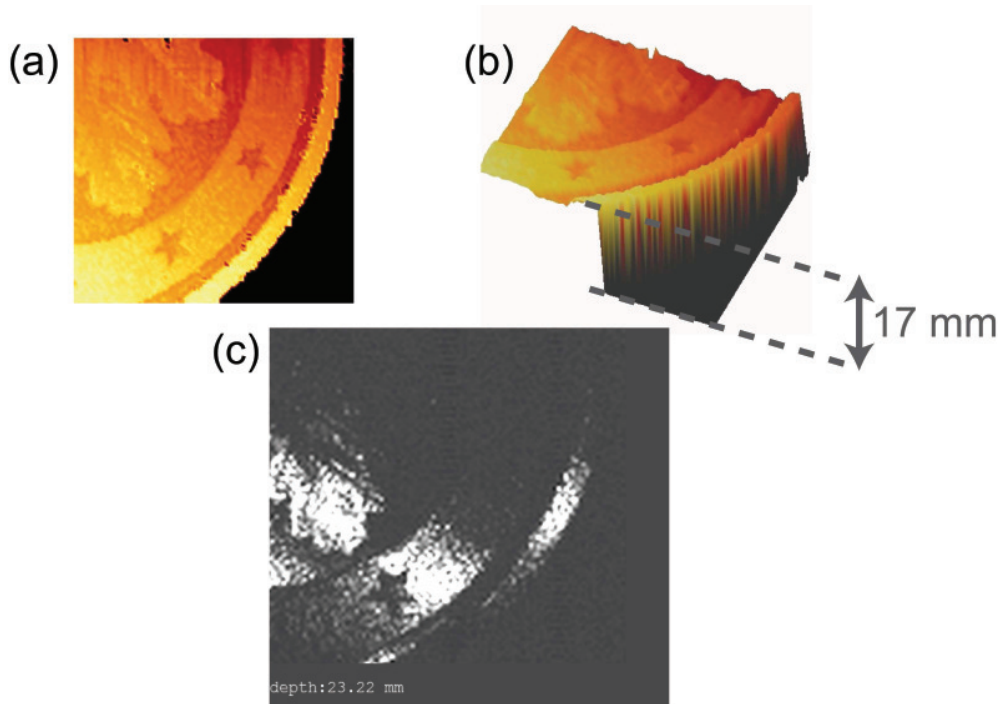


Fig. 9. Three-dimensional images of the coin surface, measured with $f_0 = 100$ Hz. (a) 2D projection of the surface profile of a two cent Euro coin. (b) 3D plot showing the same cross-section. For demonstration purposes, the distance to the ground surface is not plotted with the same z-scale as the surface profile. (c) Fly-through movie (Media 3) across 1/3 of the measured scanning range (9 mm width x 8.7 mm height x 40 mm depth).

Figure 9(a) shows a 2D projection of the coin surface, plotted using the WSxM software [32]. The depth position is encoded as intensity value. Although the overall scanning range equals 122 mm, the fine surface structures of the coin are well observable. Figure 9(b) shows a 3D projection, indicating the distance to the ground surface, measured to be 17 mm. Figure 9(c) shows a frame of the corresponding movie sequence (Media 3). The movie renders a fly through the imaged 3D-stack. The movie sequence renders only every tenth frame in the depth regions without signal, indicated by the position counter in the lower left corner. The two bright signals at the beginning of the movie represent the front- and back surfaces of a cover-slip, used as reference point for jitter correction. The coin surface appears at a depth of approximately 23 mm. The ground reflector is observable at the borders of the coin at a depth of 40 mm. Slight disturbances within the movie sequence result from multiple reflections within the scanning range.

6. Discussion

The ECOPS approach allows user adjustable scanning parameters for coherent linear optical sampling similar to classical time domain systems, but with full electronic control of the mutual time delay of the lasers. Although the scanning rate achieved in this work does not compete with scanning rates of rapid scanning optical delay lines [4–6] or spectral domain methods [33–37], both afflicted with limited scanning ranges, our technique allows to define regions of interest within large geometric extents. Further analysis of specific areas or volumes, e.g. subsurface structures, is possible by refining the electronic parameters. This allows for time and memory efficient depth scanning. This feature would require unfeasible large mechanical delay lines within the other approaches. Thus ECOPS bridges the gap between scanning range limited time domain or spectral domain systems on the one hand and large but

fixed scanning ranges achievable by ASOPS on the other hand. In contrast to ASOPS, the scanning rate can be chosen independently of the difference frequency. Thus, the approach is scalable to all laser repetition rates and the severe scanning rate limitation of ASOPS using low repetition rate lasers is removed. The advantages of flexible scanning parameters are combined with the advantages of time domain detection, namely high dynamic range by analog logarithmic amplification and the possibility to extend the method to dynamic focusing. Additionally, autocorrelation- and mirror artifacts present in spectral domain approaches [38] do not exist here.

Figures (6)–(9) demonstrate the high flexibility of electronically controlled coherent linear optical sampling. The scanning range used for the presented images varies from a few to more than 120 mm, using scanning rates between 30 and 500 Hz. The corresponding scanning velocities are within 3–12 m/s. The scanning modalities are adjustable by electronically controlling the mutual time delay between the pulses of two lasers, using a piezoelectric element within one laser cavity. The difference frequency results from the change of the cavity length, while the amount of time needed for flipping the cavity length of the slave laser above or below the cavity length of the master laser determines the maximum scanning rate. These parameters are given by the stroke and speed of the piezoelectric transducer, respectively. A stroke of 10.5 μm achievable with standard parts is sufficient here. Mechanical action within the laser cavity is only required for changing the slope of the time delay, thus the scanning rate is determined by the speed of the piezoelectric transducer, limited by the resonance frequency to a few kHz. Further enhancements in scanning rate might be possible by utilizing rapid scanning delay lines for tuning the cavity length of the slave laser. A second electronic path might be added after the balanced receiver for detecting the correlation signal during the second half cycle of triangular scanning. The carrier frequency of the second half cycle differs from the first half cycle (see Eq. (3)) and might be evaluated by a second bandpass filter and detection channel for doubling the scanning rate.

In related works, a similar change in difference frequency has been applied to ASOPS for probing carrier lifetimes [39] and for non-mechanical infrared spectroscopy [14]. However, these systems differ in terms of the electronic signal path. In these works, cavity length offsets are added after the laser stabilization circuit, modifying the difference frequency $\Delta f_{\text{REP}}(t)$ directly. If the scanning process in the positive half cycle differs from the negative half cycle, either in the absolute values of the difference frequencies or in the time interval applied for each difference frequency, the zero-point will shift due to unstabilized lasers or needs to be regulated by a low bandwidth PLL with high timing jitter [39]. Electronically controlled optical sampling avoids these disadvantages by actively controlling the direct time delay [25]. A phase value of zero forces the depth position within coherent optical sampling always to the same zero-point. The scanning scheme allows for optical sampling independent of the overall laser repetition rate and is well suited for applications demanding fiber lasers.

In contrast to our previous work [18], here the lasers are pumped by different pump sources. Furthermore, the frequency combs are not locked to reference lasers for CEO stabilization, as done in related works using fiber lasers [20]. Hence, the individual power fluctuations of these different pump sources might lead to different noise behaviour of the CEOs of both lasers. According to Eq. (3), the CEOs strongly influence the carrier frequency of the correlation signal. However, our experimental results show that simple repetition rate stabilization is sufficient to maintain reproducible signals over hours of operation. The complexity of the setup is highly reduced by avoiding the lock of the frequency combs to reference lasers. In fact, the method is stable enough to permit SNR enhancement by averaging. However, a timing jitter correction has to be performed to avoid fringe cancellation during the averaging process. Although the SNR enhancement achieved corresponds well with theoretical results, the method requires that the peak signals are already well above the noise floor to find the center positions of the correlation signals. This limitation could be removed by using a reference interferometer with fixed reflectors within the scanning range. The corresponding signals could be used to determine the individual jitter per scan and correct for these disturbances.

Further methods demonstrated by Giaccari et. al. [40] might be adapted for the presented scanning scheme.

7. Conclusion

Electronically controlled coherent linear optical sampling is a novel technique for virtually non-mechanical low coherence interferometry and optical coherence tomography. Our technique allows scanning ranges beyond the limitations of time- and spectral domain methods and scanning rates beyond the limitations of ASOPS applied to low repetition rate lasers. The limitation of equal repetition rate difference frequency and scanning rate of ASOPS is broken by applying a user adjustable phase signal to directly control the mutual time delay of two pulsed lasers. The parameters scanning range, rate and offset can be selected individually by full electronic control. The advantages of time domain systems, such as flexible scanning parameters and high dynamic range by analog logarithmic amplification, are exploited without having to accept the disadvantages of non-mechanical spectral domain methods with autocorrelation noise, mirror artifacts and scanning range vs. axial resolution limitations. Regions of interest can be defined within the samples under investigation, allowing the user to perform a time and memory efficient analysis of specific structures within a large scanning range. Applications ranging from penetration depth limited OCT imaging to remote sensing analysis of subsurface structures in three dimensions are possible with this flexible scanning scheme. This feature is especially important for the analysis of known structures, where a priori knowledge of the object might be exploited for quickly skipping unnecessary parts of the scanning range with high speed, before the region of interest is scanned in detail. Our new approach scales with the laser repetition rate and permits the use of long-cavity fiber lasers, which are highly stable and commercially available. Hence, operation beyond laboratory setups is realizable, pushing the technique to a valuable tool for precise interferometric metrology, optical coherence tomography, en-face tomographic imaging and future applications exploiting non-linear or time-dependent effects.

Acknowledgments

This work was partly supported by the Deutsche Forschungsgemeinschaft DFG, grant Fo505/2-1 and by the Interdisciplinary Centre for Clinical Research "BIOMAT" within the Faculty of Medicine at the RWTH Aachen University. We thank Toptica Photonics AG, Germany for providing the fiber lasers and the control electronics. We thank M. Lenz for scientific contributions and C. Moormann, AMO GmbH, Germany for technical support with the data acquisition system.